Suzaku and Multi-wavelength Observations of OJ 287 during the Periodic Optical Outburst in 2007

Hiromi Seta, [1] Naoki Isobe, [2] Makoto S. Tashiro, [1] Yuichi Yaji, [1]
Akira Arai, [3] Masayuki Fukuhara, [4,5] Kotaro Kohno, [6] Koichiro Nakanishi, [5]
Mahito Sasada, [3] Yoshito Shimajiri, [4,5] Tomoka Tosaki, [5] Makoto Uemura, [7]
and
H Anderhub, [8] L A. Antonelli, [9] P Antoranz, [10] M Backes, [11] C Baixeras, [12]
S Balestra, [10] J A. Barrio, [10] D Bastieri, [13] J Becerra González, [14] J K. Becker, [11]
W Bednarek, [15] K Berger, [15] E Bernardini, [16] A Biland, [8] R K. Bock, [17,13]
G Bonnoli, [18] P Bordas, [19] D Borla Tridon, [17] V Bosch-Ramon, [19] D Bose, [10]
I Braun, [8] T Bretz, [20] I Britvitch, [8] M Camara, [10] E Carmona, [17] S Commichau, [8]
J L. Contreras, [10] J Cortina, [21] M T. Costado, [14,22] S Covino, [9] V Curtef, [11]
F Dazzi, [23,35] A. De Angelis, [23] E De Cea del Pozo, [24] R de los Reyes, [10]
B De Lotto, [23] M De Maria, [23] F De Sabata, [23] C Delgado Mendez, [14,32]
A Dominguez, [25] D Dorner, [8] M Doro, [13] D Elsaesser, [20] M Errando, [21]
D Ferenc, [26] E Fernández, [21] R Firpo, [21] M V. Fonseca, [10] L Font, [12] N Galante, [17]
R J. García López, [14,22] M Garczarczyk, [21] M Gaug, [14] F Goebel, [17,36] D Hadasch, [12]
M Hayashida, [17,33] A Herrero, [14,22] D Hildebrand, [8] D Höhne-Mönch, [20] J Hose, [17]
C C. Hsu, [17] T Jogler, [17] D Kranich, [8] A La Barbera, [9] A Laille, [26] E Leonardo, [18]
E Lindfors, [27] S Lombardi, [13] F Longo, [23] M López, [13] E Lorenz, [8,17] P Majumdar, [16]
G Maneva, [28] N Mankuzhiyil, [23] K Mannheim, [20] L Maraschi, [9] M Mariotti, [13]
M Martínez, [21] D Mazin, [21] M Meucci, [18] M Meyer, [20] J M. Miranda, [10]
R Mirzoyan, [17] H Miyamoto, [17] J Moldón, [19] M Moles, [25] A Moralejo, [21] D Nieto, [10]
K Nilsson, [27] J Ninkovic, [17] N Otte, [17,34] I Oya, [10] R Paoletti, [18] J M. Paredes, [19]
M Pasanen, [27] D Pascoli, [13] F Pauss, [8] R G. Pegna, [18] M A. Perez-Torres, [25]
M Persic, [23,29] L Peruzzo, [13] F Prada, [25] E Prandini, [13] N Puchades, [21]
I Reichardt, [21] W Rhode, [11] M Ribó, [19] J Rico, [30,21] M Rissi, [8] A Robert, [12]
S Rügamer, [20] A Saggion, [13] T Y. Saito, [17] M Salvati, [9] M Sanchez-Conde, [25]
K Satalecka, [16] V Scalzotto, [13] V Scapin, [23] T Schweizer, [17] M Shayduk, [17]
S N. Shore, [31] N Sidro, [21] A Sierpowska-Bartosik, [24] A Sillanpää, [27] J Sitarek, [17,15]
D Sobczynska, [15] F Spanier, [20] A Stamerra, [18] L S. Stark, [8] L Takalo, [27]
F Tavecchio, [9] P Temnikov, [28] D Tescaro, [21] M Teshima, [17] M Tluczykont, [16]
D F. Torres, [30,24] N Turini, [18] H Vankov, [28] R M. Wagner, [17] W Wittek, [17]
V Zabalza, [19] F Zandanel, [25] R Zanin, [21] J Zapatero [12]
(The MAGIC Collaboration)

[1]*Department of Physics, Saitama University, 255 Shimo-Okubo, Sakura, Saitama 338-8570*
seta@heal.phy.saitama-u.ac.jp
[2]*Department of Astronomy, Kyoto University, Kitashirakawa-Oiwakecho, Sakyo-ku, Kyoto 606-8502*
[3]*Department of Physical Science, Hiroshima University, 1-3-1 Kagamiyama, Higashi-Hiroshima 739-8526*
[4]*Department of Astronomy School of Science, University of Tokyo, Bunkyo, Tokyo 113-0033*
[5]*Nobeyama Radio Observatory, Minamimaki, Minamisaku, Nagano 384-1305*
[6]*Institute of Astronomy, The University of Tokyo, 2-21-1 Osawa, Mitaka, Tokyo 181-0015*
[7]*Astrophysical Science Center, Hiroshima University, 1-3-1 Kagamiyama, Higashi-Hiroshima 739-8526*
[8]*ETH Zurich, CH-8093 Switzerland*
[9]*INAF National Institute for Astrophysics, I-00136 Rome, Italy*
[10]*Universidad Complutense, E-28040 Madrid, Spain*
[11]*Technische Universität Dortmund, D-44221 Dortmund, Germany*
[12]*Universitat Autònoma de Barcelona, E-08193 Bellaterra, Spain*
[13]*Università di Padova and INFN, I-35131 Padova, Italy*
[14]*Inst. de Astrofísica de Canarias, E-38200 La Laguna, Tenerife, Spain*
[15]*University of Łódź, PL-90236 Lodz, Poland*
[16]*Deutsches Elektronen-Synchrotron (DESY), D-15738 Zeuthen, Germany*
[17]*Max-Planck-Institut für Physik, D-80805 München, Germany*
[18]*Università di Siena, and INFN Pisa, I-53100 Siena, Italy*
[19]*Universitat de Barcelona (ICC/IEEC), E-08028 Barcelona, Spain*
[20]*Universität Würzburg, D-97074 Würzburg, Germany*
[21]*IFAE, Edifici Cn., Campus UAB, E-08193 Bellaterra, Spain*
[22]*Depto. de Astrofisica, Universidad, E-38206 La Laguna, Tenerife, Spain*
[23]*Università di Udine, and INFN Trieste, I-33100 Udine, Italy*
[24]*Institut de Cienciès de l'Espai (IEEC-CSIC), E-08193 Bellaterra, Spain*
[25]*Inst. de Astrofísica de Andalucia (CSIC), E-18080 Granada, Spain*
[26]*University of California, Davis, CA-95616-8677, USA*
[27]*Tuorla Observatory, University of Turku, FI-21500 Piikkiö, Finland*
[28]*Inst. for Nucl. Research and Nucl. Energy, BG-1784 Sofia, Bulgaria*
[29]*INAF/Osservatorio Astronomico and INFN, I-34143 Trieste, Italy*
[30]*ICREA, E-08010 Barcelona, Spain*
[31]*Università di Pisa, and INFN Pisa, I-56126 Pisa, Italy*
[32]*now at: Centro de Investigaciones Energ ticas, Medioambientales y Tecnol gicas (CIEMAT), Madrid, Spain*
[33]*now at: SLAC National Accelerator Laboratory and KIPAC, CA, 94025, USA*
mahaya@slac.stanford.edu

[34] *now at: University of California, Santa Cruz, CA 95064, USA*
[35] *supported by INFN Padova*
[36] *deceased*

(Received 2009 0; accepted 2009 0)

Abstract

Suzaku observations of the blazar OJ 287 were performed in 2007 April 10 – 13 and November 7 – 9. They correspond to a quiescent and a flaring state, respectively. The X-ray spectra of the source can be well described with single power-law models in both exposures. The derived X-ray photon index and the flux density at 1 keV were found to be $\Gamma = 1.65 \pm 0.02$ and $S_{1\mathrm{keV}} = 215 \pm 5$ nJy, in the quiescent state. In the flaring state, the source exhibited a harder X-ray spectrum ($\Gamma = 1.50 \pm 0.01$) with a nearly doubled X-ray flux density $S_{1\mathrm{keV}} = 404^{+6}_{-5}$ nJy. Moreover, significant hard X-ray signals were detected up to ~ 27 keV. In cooperation with the Suzaku, simultaneous radio, optical, and very-high-energy γ-ray observations of OJ 287 were performed with the Nobeyama Millimeter Array, the KANATA telescope, and the MAGIC telescope, respectively. The radio and optical fluxes in the flaring state (3.04 ± 0.46 Jy and 8.93 ± 0.05 mJy at 86.75 Hz and in the V-band, respectively) were found to be higher by a factor of 2 – 3 than those in the quiescent state (1.73 ± 0.26 Jy and 3.03 ± 0.01 mJy at 86.75 Hz and in the V-band, respectively) . No notable γ-ray events were detected in either observation. The spectral energy distribution of OJ 287 indicated that the X-ray spectrum was dominated by inverse Compton radiation in both observations, while synchrotron radiation exhibited a spectral cutoff around the optical frequency. Furthermore, no significant difference in the synchrotron cutoff frequency was found between the quiescent and flaring states. According to a simple synchrotron self-Compton model, the change of the spectral energy distribution is due to an increase in the energy density of electrons with small changes of both the magnetic field strength and the maximum Lorentz factor of electrons.

Key words: BL Lacertae objects: general — BL Lacertae objects: individual (OJ 287) — radiation mechanisms: non-thermal — X-rays: galaxies

1. Introduction

At a redshift of $z = 0.306$ (Stickel et al. 1989), OJ 287 is one of the archetypal and most studied blazars. An outstanding characteristic of the object is its recurrent optical outbursts with a period of 11.65 years, as revealed by optical data spanning more than 100 years (Sillanpää et al. 1988). The outburst in 1994 motivated a worldwide multi-wavelength observa-

tion campaign named "The OJ 94 project" (Sillanpää et al. 1996a). This project confirmed the periodicity and revealed that the optical outbursts consist of two peaks corresponding to flares with an interval of about one year (Sillanpää et al. 1996b). OJ 287 is suggested to be a binary black hole system in which a secondary black hole pierces the accretion disk of the primary black hole and produces two impact flushes per period (Valtonen et al. 2008a). Interestingly, the first flare exhibited a low radio flux with decreasing radio polarization and a relatively short duration (a few months), while the second one had a high radio flux with increasing radio polarization, and lasted about half a year (Sillanpää et al. 1996b; Valtaoja et al. 2000; Pursimo et al. 2000). The differences between the two flares may be interpreted as the first flare have a thermal origin in the vicinity of the black hole and the accretion disk, while the second one originate from synchrotron radiation from the jet (Valtaoja et al. 2000), although we have not yet obtained any convincing evidence supporting this interpretation.

The multi-wavelength spectral energy distribution (SED) has the potential to resolve the physical state of OJ 287 during the flares. In general, the SED of blazars is characterized by two broad humps (e.g., Fossati et al. 1998); the low-energy component, with wavelengths in the range between radio to ultraviolet and X-ray, is widely regarded as synchrotron radiation (SR) from relativistic electrons within the jet. The high-energy component, with wavelengths in the range between X-rays and γ-rays, is interpreted as inverse-Compton (IC) scattering. In one of the simple emission models, named "synchrotron self-Compton (SSC) model", relativistic electrons scatter SR photons produced by the same population of electrons (e.g., Ghisellini et al. 1998). For low-frequency peaked BL Lac objects (LBLs), a class of blazars to which OJ 287 belongs, the SR peak is located in the range between sub-mm and optical wavelengths (Padovani & Giommi 1995). IC scattering in LBLs can emit radiation up to very-high-energy (VHE: E>50 GeV) γ-rays during their optical high states; VHE γ-ray emission has been detected, for example, from BL Lacertae (Albert et al. 2007) and S5 0716+714 (Teshima et al. 2008). These two components usually intersect with each other in the X-ray band (e.g., Giommi et al. 1999). Therefore, the X-ray spectrum of LBLs should be highly sensitive to the change of the magnetic field (B) and/or the maximum Lorentz factor ($\gamma_{\rm max}$) of the electrons, since the SR peak scales as $\propto B\gamma_{\rm max}^2$. In fact, the X-ray spectrum of the object, obtained in previous observations, can be successfully interpreted on the basis of the interplay between the SR and the IC component (Idesawa et al. 1997; Isobe et al. 2001). However, all of these X-ray observations were carried out during the first flare, and there is no information regarding the X-ray spectrum of OJ 287 in the second flare.

In the period between 2005 and 2008, OJ 287 was predicted to move to the last active phase, and was in fact reported to exhibit the first optical outburst in 2005 November (Valtonen et al. 2008a; Valtonen et al. 2008b). Since the second flare of the source was expected to be in the fall of 2007 (Valtonen et al. 2006; Kidger 2000), we organized two X-ray and simultaneous multi-wavelength observations, in the quiescent state (MWL I) between the two outbursts

and in the second flaring state (MWL II), with the objective to reveal the characteristics of the second flare, in comparison with the quiescent state. Based on the results, we provide a discussion regarding the differences between the first and the second flare. The Suzaku X-ray observation in MWL I was conducted during 2007 April 10 – 13, when the source was optically quiescent with an R-band magnitude of about 15. We triggered the MWL II Suzaku observation in 2007 November 7, on condition that the object remained brighter than 14-th magnitude for more than one week, as indicated by the optical monitoring data of the source taken at the Tuorla Observatory and the KVA observatory [1]. We also conducted monitoring observations at radio, optical, and VHE γ-ray frequencies with the Nobeyama Millimeter Array (NMA), the KANATA telescope, and the MAGIC telescope, respectively.

The X-ray observations and the spectral results are presented in section 2. section 3 shows the radio, optical, and VHE γ-ray results. These are followed by the discussion on the physical state of the second flare in section 4 on the basis of SED obtained in these multi-frequency observations.

2. X-ray Observations and Results

2.1. Observations and data reduction

The Suzaku pointing observation for MWL I was conducted between 19:47:00 UT 2007 April 10 and 11:10:19 UT April 13 (ObsID 702009010), and the pointing for MWL II was conducted between 11:24:00 UT 2007 November 7 and 21:30:23 November 9 (ObsID 702008010). The X-ray Imaging Spectrometer (XIS; Koyama et al. 2007) and the Hard X-ray Detector (HXD; Takahashi et al. 2007; Kokubun et al. 2007) onboard Suzaku were operated in the normal clocking mode with no window option, and in the normal mode, respectively.

We placed OJ 287 at the HXD-nominal position (Serlemitsos et al. 2007). We performed data reduction by using the HEADAS 6.5.1 software package and referring to the calibration data base (CALDB) of the XIS, the X-ray telescope (XRT; Serlemitsos et al. 2007), and the HXD as of 2008 September 5, 2008 July 9, and 2008 August 11, respectively.

We reprocessed the XIS data in MWL I since the version of the standard processing (Revision 2.0.6.13) was obsolete, whereas we utilized the pipeline cleaned events from the Revision 2.1.6.16 processing for MWL II. The reprocessed/cleaned XIS data were filtered under the following criteria; the spacecraft is outside the south Atlantic anomaly (SAA), the time interval after an exit from the SAA is longer than 436 s, the geomagnetic cutoff rigidity (COR) is higher than 6 GV, the source elevation above the rim of bright and night Earth (ELV) is higher than 20° and 5°, respectively, and the XIS data are free from telemetry saturation. These procedures yielded 85.3 ks and 102.6 ks of good exposures, for MWL I and MWL II. In the scientific analysis below, we utilize only the events with grades of 0, 2, 3, 4, or 6.

[1] http://users.utu.fi/kani/1m/OJ_287_jy.html

We reprocessed the HXD data in both observations by using the latest gain file in the CALDB. The HXD data were screened under the following criteria; the time interval before and after the SAA is longer than 180 s and 500 s, COR and ELV are higher than 6 GV and 5°, respectively. As a result, we obtained 93.6 ks and 102.9 ks of good exposures, for MWL I and MWL II.

2.2. XIS Results

Figure 1 shows the 0.5 – 10 keV XIS images in MWL I and MWL II. OJ 287 was clearly detected at the position of $(\alpha, \delta) = (08^{\rm h}54^{\rm m}48\overset{\rm s}{.}87,\ 20°06'30\overset{''}{.}6)$ in J2000.0 coordinates, with no other apparent contaminating source within the XIS field of view. The image indicates that the intensity of the source was higher in MWL II than in MWL I. We accumulated the source signals within the solid circles with a radius of $3'$ in figure 1. The background events were integrated within the same radius (dashed circles) at symmetric positions around the optical axis of the XRT.

In figure 2, we show the background-subtracted X-ray lightcurves of OJ 287 in MWL I and MWL II. The data from the two front-illuminated (FI) CCD cameras (XIS 0 and 3; Koyama et al. 2007) were co-added. In MWL I, the time-averaged count rates in the soft (0.5 – 2 keV) and medium (2 – 10 keV) bands were measured to be 0.088 ± 0.001 cts s^{-1} and 0.071 ± 0.001 cts s^{-1}, respectively, while they nearly doubled to 0.166 ± 0.001 cts s^{-1} and 0.164 ± 0.002 cts s^{-1} in MWL II. With $\chi^2 = 42.9$ and 27.7 for 39 degrees of freedom (d.o.f.), the lightcurve indicates no significant variation during MWL I in either energy band. On the other hand, in MWL II, we found that the source flux gradually decreased by a factor of 1.3 in the first half of the observation (~ 1.5 days; χ^2/d.o.f. $= 58.5/37$ and $71.3/37$ in the soft and medium bands). However, the hardness ratio, which was simply calculated by dividing the count rate of the medium band by that of the soft band, indicates no significant spectral variation in either observation. Therefore, we evaluated the averaged spectra as presented below.

Figure 3 shows the background-subtracted XIS spectra of OJ 287, without removing the instrumental response. In this case, significant X-ray signals were detected in the range of 0.5 – 10 keV and 0.4 – 8 keV, with the FI CCDs and the backside-illuminated (BI) CCD (XIS 1). The spectra appear to be featureless, without any absorption or emission lines.

We fitted the spectra with a single power-law (PL) model modified for photoelectric absorption and subsequently calculated the response matrix function and the auxiliary response file by using `xisrmfgen` and `xissimarfgen` (Ishisaki et al. 2007), respectively. The effects of absorption caused by the presence of contaminants on the surface of the optical blocking filter of the CCD is taken into account in `xissimarfgen`. The FI and BI spectra were jointly fitted by allowing deviations between their respective model normalizations. Because we found that the fluxes from the BI and FI spectra were in good agreement within 7 %, we adopt the FI value in the present paper. We fixed the absorption column density at the Galactic value

($N_{\rm H} = 2.56 \times 10^{20}$ cm^{-2}; Kalberla et al. 2005). The PL model became acceptable, yielding the best-fit photon index of $\Gamma = 1.65 \pm 0.02$ and $\Gamma = 1.50 \pm 0.01$ for MWL I and MWL II, respectively. Thus, we found that OJ 287 showed a harder X-ray spectrum in MWL II. As indicated in the lightcurve (figure 2), the flux density of the source in MWL II (404^{+6}_{-5} nJy) was higher than that in MWL I (215 ± 5 nJy) by a factor of 2.

2.3. HXD-PIN Results

It is crucial to evaluate the non-X-ray background (NXB), before examining the hard X-ray spectrum observed with the HXD-PIN (Takahashi et al. 2007; Kokubun et al. 2007). Although the NXB varies under various cosmic ray environments in the orbit, the HXD team revealed a set of control parameters for reproducing the NXB and supplied simulated NXB event files for each observation. The latest version of the NXB model, named "tuned"-NXB (LCFITDT in Fukazawa et al. 2009), was reported to have a systematic reproducibility error of 2.31 % and of 0.99 % with 10 ks and 40 ks exposures, respectively, in the 15 – 40 keV band.

First, we analyzed the HXD-PIN data in MWL I. Since the data during Earth occultation is essentially dominated by the NXB events, these data allow for the reproducibility of the NXB model to be evaluated. The data were obtained with the same criteria as in the case of the on-source observation (section 2.1), with the exception that ELV $< -5^\circ$ instead of ELV $> 5^\circ$. The exposure of 44.1 ks was attained under these conditions. Figure 4 (a) compares the observed Earth-occultated (black), the NXB model (red), and the NXB-subtracted (green) spectra. Table 2 summarizes the statistics of the data and the NXB model in MWL I. We found a data excess of 3.8 ± 1.0 % over the NXB model below 20 keV. The apparent excess below 20 keV is within a 3 σ level of the current uncertainty of the NXB model (Fukazawa et al. 2009). Therefore, we consider that the excess is an artifact produced by fluctuations in the NXB model. In other words, the NXB model underestimates the real NXB data with ~ 4 % in this observation. It is necessary to take this into account for the on-source data.

In a similar manner, we compared the on-source and NXB model spectra, and the results are shown in figure 4 (b). We found a significant data excess over the NXB model, in the 12 – 40 keV range. This excess includes not only the source signals, but also those of the cosmic X-ray background (CXB). In order to evaluate the CXB component, we introduced the CXB spectrum within the HXD field of view as

$$F(E) = (9.412 \times 10^{-3}) \Big(\frac{E}{1\mathrm{keV}} \Big)^{-1.29} \exp\Big[\frac{-E}{40\mathrm{keV}} \Big] \text{ photons s}^{-1}\text{cm}^{-2}\text{keV}^{-1},$$

in accordance to Boldt (1987). We folded this spectrum with the HXD-PIN response of `ae_hxd_pinhxnome3_20080129.rsp` which was appropriate to the observation phase (Epoch 3), and show it in figure 4 (b). We also summarized the statistics of the data, the NXB, and the CXB in table 3. The NXB count rate for on-source is higher than that for the Earth occultation, due to different orbit conditions of the satellite, as can be seen in tables 2 and

3. Therefore, it is of no use to perform a direct comparison of the count rates between the Earth occultation and on-source periods, and therefore we examined the ratio of the combined NXB and CXB to the NXB. After subtracting the CXB and NXB models, the on-source data corresponded to 4.2 ± 0.3 % and -0.9 ± 0.2 % of the NXB, in 12 – 20 keV and 20 – 40 keV, respectively. By using the Earth occultation data, we ascribed the apparent excess in 12 – 20 keV due to the uncertainly of the NXB model instead of the source signals since we confirmed that the NXB model underestimates the real NXB spectrum by ~ 4 %.

Next, in (a) in figure 5, we show the HXD-PIN spectra of MWL II during the Earth occultation with an exposure of 28.7 ks. Table 3 summarizes the statistics of the data and the NXB model during the Earth occultation. They are consistent with each other within 1.4 ± 1.2% and 1.2 ± 1.6% in 12 – 20 keV and 20 – 40 keV. Thus, we confirmed that the NXB model adequately reproduced the observed NXB spectrum in MWL II within its reported uncertainty.

Figure 5 (b) shows the on-source spectra in MWL II. In order to fold the CXB spectra, we used the HXD-PIN response function (Epoch 4), `ae_hxd_pinhxnome4_20080129.rsp`. The HXD-PIN spectrum revealed a significant excess over the combined CXB and NXB in the 12 – 27 keV range. The count rates for the data, the NXB and the CXB in this range, are shown in table 3. Thus, the excess has a count rate of 0.011 ± 0.002 cts s^{-1} (2.9 ± 0.6 % of the NXB), which corresponds to statistical significance of 5.0σ. Since this is well above the NXB errors, we concluded that the HXD-PIN detected signals from OJ 287 in MWL II.

Due to the rather low signal statistics of the HXD-PIN in comparison to the XIS, instead of joint fitting of XIS and HXD-PIN spectra, we compared the flux of the HXD-PIN signal to the fitting result of the XIS spectrum. The simple extrapolation of the best-fit single PL model to the XIS spectrum (section 2.2) has a count rate of 0.016 cts s^{-1} in 12 – 27 keV, after the correction of the relative normalization of the HXD to the XIS (1.14: Ishida et al. 2007). The detected HXD-PIN count rate is only 0.65 times this value, which suggests the presence of a spectral break between the XIS and the HXD-PIN range, although it is statistically insignificant (2.6 σ).

3. Multi-wavelength Observations and Results

3.1. Radio Observations

Eleven radio observations of OJ 287 with the NMA at the Nobeyama Radio Observatory were carried out between January 2007 and January 2008. The NMA consists of six 10-m antennas equipped with cooled DSB SIS receivers. An Ultra-Wide-Band Correlator (Okumura et al. 2000) was employed as the spectrocorrelator. We performed simultaneous observations of a radio continuum emission from OJ 287 at 86.75 GHz and 98.75 GHz, with a 1 GHz bandwidth for each band. The total on-source time of OJ 287 in each observation was between

nine and twelve minutes. In each observation session, OJ 287 and the bright reference amplitude calibrators (3C 84 or 3C 345) were observed alternately. The relative amplitude ratios between OJ 287 and these reference calibrators were obtained from the visibility data. As absolute flux-scale calibrations, Uranus or Neptune was used in order to calculate the final flux values of OJ 287. The uncertainties in the absolute flux scale were estimated to be about 15 % for each observation, taking into account statistical errors induced by noise and systematic errors caused by flux fluctuations of the reference calibrators.

For MWL I, we observed the source on 11 and 12 April, overlapping with the Suzaku pointing. The averaged flux of the two night observations was 1.73 ± 0.26 Jy and 1.75 ± 0.26 Jy at 86.75 GHz and 98.75 GHz, respectively. During the period of MWL II, the observations on November 7 and 8 were coincident with the Suzaku pointing. The averaged flux of the two day observations was 3.04 ± 0.46 Jy and 2.98 ± 0.45 Jy at 86.75 GHz and 98.75 GHz, respectively (see table 4). The measured radio flux for MWL II was 1.7 – 1.8 times higher than that for MWL I.

3.2. Optical Observations

Optical and near-infrared (NIR) photometric observations were performed at the Higashi-Hiroshima Observatory with the 1.5-m "KANATA" telescope. We obtained images of the field of OJ 287 with V, J, and K_s filters by using TRISPEC attached to the telescope (Watanabe et al. 2005). The V-band images were observed for 53 nights between 2006 October and 2007 December. For each night, we obtained ~ 20 images with an exposure time of 108 s for each frame. The magnitude of OJ 287 was measured by differential photometry with a neighbor comparison star located at $(\alpha, \delta) = (08^{\rm h}54^{\rm m}52\overset{\rm s}{.}7,\ 20^\circ04'46'')$. The V-magnitude of the comparison star ($V = 14.160$) was quoted from Skiff (2007). After preparing dark-subtracted and flat-fielded images, we measured the magnitudes of the objects by using the aperture photometry package in IRAF. We also checked the constancy of the comparison star by using a neighbor star at $(\alpha, \delta) = (08^{\rm h}54^{\rm m}59\overset{\rm s}{.}0,\ 20^\circ02'58'')$. The differential magnitude of the comparison star exhibited no significant fluctuation exceeding 0.003-th during our observations.

We also obtained NIR images, for MWL I on 2007 April 11, 12, and 13, as well as for MWL II on November 7, 8, and 10, which overlapped with the Suzaku pointing. Simultaneous V, J, and K_s-band images are available for these six nights. The exposure times of each frame were 15 and 4 s for the J and K_s-band images, respectively. The reduction procedure was similar to that in the V-band data mentioned above, and we used the same comparison stars and target stars as those for the V-band data. The J and K_s magnitudes of the comparison star were quoted from the 2MASS catalog ($J = 12.664$ and $K_s = 12.090$; Skrutskie et al. 2006). We confirmed that the magnitude of the comparison star remained constant within 0.004 and 0.012-th for J and K_s-bands during our observations. In MWL I, the averaged flux of three night observations was 3.03 ± 0.01 mJy, 8.81 ± 0.03 mJy, and 17.74 ± 0.33 mJy for V, J, K_s-

band, respectively. In MWL II, these fluxes were 8.93 ± 0.05 mJy, 27.02 ± 0.21 mJy, and $55.95^{+7.96}_{-6.76}$ mJy, respectively. (see table 4). It can be seen that the source flux for MWL II is higher by a factor 3 as compared to that for MWL I. The optical data show a monotonous decrease in a time scale of ~ 4 days during MWL II by a factor of 1.3.

In addition, we obtained R-band frames from the KVA Telescope simultaneously with Suzaku pointings. The exposure time was 180 s for each frame. Photometric measurements were conducted in differential mode, that is, by obtaining CCD images of the target and the calibrated comparison stars in the same field of view (Fiorucci & Tosti 1996). The magnitudes of the source and the comparison stars were measured using aperture photometry and the (color-corrected) zero point of the image as determined from the magnitude of the comparison star. Finally, the object magnitude was computed using the zero point and a filter-dependent color correction. After this, magnitudes were transferred into linear fluxes by using the formula $F = F_0 \times 10^{(mag/-2.5)}$, where mag is the magnitude of the object and F_0 is a filter-dependent zero point (the value $F_0 = 3080$ Jy is used in the R-band, Bessell 1979).

3.3. VHE γ-ray Observations

We used the MAGIC telescope to search for VHE γ-rays emission from OJ 287 during the MWL campaigns I and II. MAGIC is a single dish Imaging Atmospheric Cherenkov Telescope (IACT) with a 17-m diameter main reflector. The telescope is located in the Canary Island of La Palma, in regular operation since 2004 with a low energy threshold of 50 – 60 GeV (trigger threshold at small zenith angles; Albert et al. 2008a).

In MWL I, MAGIC observed during 3 nights. The zenith angle of the observations ranges from 8° to 29°. The observations were performed in so-called ON-OFF observation mode. The telescope was pointing directly to the source, recording ON-data. The background was estimated from additional observations of regions where no γ-ray is expected, OFF-data, which were taken with sky conditions similar to ON-data. Data runs with anomalous trigger rates due to bad observation conditions were rejected from the analysis. The remaining data correspond to 4.5 hours of ON and 6.5 hours of OFF data. In November and December 2007 for MWL II, MAGIC observed in a zenith angle range from 8° to 31° in the "wobble mode" (Fomin et al. 1994), where the object was observed at 0.4° offset from the camera center. With this observation mode, an ON-data sample and OFF-data samples can be extracted from the same observation run; in our case, we used 3 OFF regions to estimate the background. In total, the data were taken during 22 nights, two of which coincide with the Suzaku pointing. 41.2 hours of data from 19 nights passed the quality selection to be used for further analysis.

The VHE γ-ray data taken for MWLs I and II were analyzed using the MAGIC standard calibration and analysis software. Detailed information about the analysis chain is found in Albert et al. (2008a). In February 2007, the signal digitization of MAGIC was upgraded to 2 GSamples s^{-1} FADCs, and timing information is used to suppress the contamination of light

of the night sky and to obtain new shower image parameters (Aliu et al. 2009) in addition to conventional *Hillas* image parameters (Hillas 1985).

These parameters were used for γ/hadron separation by means of the "Random Forest (RF)" method (Albert et al. 2008b). The γ/hadron separation based on the RF method was turned to give a γ-cut efficiency of 70 %. Finally, the γ-ray signal was determined by comparing between ON and normalized-OFF data in the —ALPHA— parameter[2] distribution, in which the γ-ray signal should show up as an excess at small values. Our analysis requires a γ-cut efficiency of 80 % for the final —ALPHA— selection. The energy of the γ-ray events are also estimated using the RF method.

A search of VHE γ-rays from OJ 287 was performed with data taken for MWLs I and II in three distinct energy bins. No significant excess was found in any data samples. Upper limits with 95 % confidence level in the number of excess events were calculated using the method of Rolke et al. (2005), taking into account a systematic error of 30 %. The number of excess events was converted into flux upper limits assuming a photon index of -2.6, corresponding to the value used in our Monte-Carlo samples of γ-rays. The derived upper limits in the three energy bins for each period are summarized in table 5.

A search for VHE flares with a short-time scale was also performed with the data taken for MWL II. Figure 6 shows the nightly count rate of the excess events after all cuts including a SIZE cut above 200 photoelectrons, corresponding to an energy threshold of 150 GeV. Fitting a constant rate to the observed flux yields $\chi^2/\mathrm{d.o.f.} = 25.55/18$ (a probability of 11 %), and thus indicates no evidence of a VHE flare during this period.

4. Discussion

We performed Suzaku X-ray observations of OJ 287 in the quiescent state (MWL I) and the second flare (MWL II) in 2007 April and November, respectively, where the latter was the first X-ray observation during the second flare of the source. In cooperation with Suzaku, radio, optical, and VHE γ-ray observations were performed with NMA, KANATA, and MAGIC, respectively. Figure 7 summarizes the multi-wavelength lightcurves obtained between September 2006 and January 2008. While the optical flux of OJ 287 was below 3 mJy in the V-band before MWL I, the brightness of the source started increasing after MWL I to become the flaring state ($\gtrsim 7$ mJy) in September 2007. Although the radio flux gradually decreased around the period of MWL I, it started increasing during the optical flare in MWL II, and it also increased in other energy bands. We found that the brightness of the source increased by a factor of 2 – 3, in the radio, optical, and X-ray bands between MWL I and MWL II, although no significant VHE γ-ray signals were detected in either MWL I or MWL II.

[2] the angle between the shower image principal axis and the line connecting the image center of gravity with the camera center.

As shown in figure 3, significant X-ray signals were detected with the XIS in the range 0.5 – 10 keV range. The HXD-PIN detected hard X-ray signals in 12 – 27 keV with a significance of 5.0 σ in MWL II (figure 5), while those signals were not significant in MWL I (figure 4). The XIS spectra in 0.5 – 10 keV were described with a single PL model modified with Galactic absorption in MWL I and MWL II. The photon indices and the flux densities at 1 keV were derived as 1.65 ± 0.02 and 215 ± 5 nJy in MWL I, and 1.50 ± 0.01 and 404^{+6}_{-5} nJy in MWL II.

In the previous observations of the first flares and quiescent states, the X-ray flux densities at 1 keV and photon indices of OJ 287 were estimated as 0.15 – 0.31 μJy and 1.45 – 1.63, respectively, in 1997 – 2001 with BeppoSAX (Massaro et al. 2003), 0.22 – 0.25 μJy and 1.51 – 1.57 in 1997 with ASCA (Isobe et al. 2001), $0.76\ ^{+0.03}_{-0.06}$ μJy and 1.67 ± 0.02 in 1994 with ASCA (Idesawa et al. 1997), 2.08 – 2.24 μJy and 2.16 – 2.37 in 1983 – 1984 with EXOSAT (Sambruna et al. 1994), and 0.94 – 2.70 μJy and 1.5 – 2.3 in 1979 – 1980 with Einstein satellite (Madejski & Schwartz 1988). These results suggest that the X-ray spectrum became softer as the source became brighter (Idesawa et al. 1997; Isobe et al. 2001). This trend was interpreted in the following way: during the quiescent state, the IC component dominates the X-ray spectrum (Isobe et al. 2001). However, once the X-ray flux increases, the high-frequency end of the SR component extends to the X-ray band and exhibits a softer spectrum. In fact, Isobe et al. (2001) have successfully decomposed the X-ray spectrum obtained with ASCA at the first flare in 1994 into soft and hard PL components representing the SR and the IC components, respectively. Moreover, in the XMM-Newton observation of the recent first flare in 2005, the source exhibited a concave broken-PL-like X-ray spectrum (Ciprini et al. 2008) which also supports the idea that there is a contribution from the soft component. On the other hand, the spectral behavior in the second flare of OJ 287 observed with Suzaku was completely the opposite to the previous X-ray trend in the first flares.

In order to perform a quantitative evaluation of the possible soft excess component in the Suzaku X-ray spectrum obtained in MWL II, we employed an additional steep PL model modified with the Galactic absorption. The photon index of the additional steep PL component was fixed at 2.62, which is the best fit value for the first flare in 1994 (Isobe et al. 2001), while its normalization was left free. As a result of this two-component model fitting, the upper limit on the flux density of the additional soft PL component was derived as 8.7 nJy at the 3σ level (see table 1), while the hard component remained consistent with the best fit values for the single PL model fitting (χ^2/d.o.f. $= 566.4/519$). Thus, we obtained the upper limit on the ratio of the soft to the hard components at 1 keV as 0.022, although the ratio was estimated to be 0.186 ± 0.034 in the first flare of 1994 (Isobe et al. 2001). Therefore, the contribution from the soft component in MWL II was negligible in comparison to that of the first flare, and the hard component fully dominated the XIS spectrum over the 0.5 – 10 keV range.

Figure 8 shows the overall SED of OJ 287 for the Suzaku pointing in MWL I and MWL II, including the optical R-band data from the KVA Telescope, as well as some historical data.

In the figure, we recognize two spectral components, which are typical of blazars. The low frequency SR component, extending from radio to optical frequencies, has a spectral turnover at around 5×10^{14} Hz. At the same time, the observed SR component is well above the extrapolation from the upper limit of the soft PL component in MWL II ($\sim 1 \times 10^{-12}$erg s^{-1} cm^{-2} at 5×10^{14} Hz). Therefore, we naturally attribute the observed hard X-ray spectrum to the IC component rising toward the higher frequency range. The SED indicates that both the SR and IC intensities increased from MWL I to MWL II without any significant shift of the SR peak frequency.

As a working hypothesis, here we assume simply that the variation of the SED was caused by a change in electron energy density (or number density) and/or the maximum Lorentz factor of the electrons, with stable magnetic field, volume of emission region, minimum Lorentz factor, and break of electron energy distribution (e.g., Takahashi et al. 2000). In order to evaluate this hypothesis, we applied a one-zone SSC model to the SED by using the numerical code developed by Kataoka (2000). The electron number density spectrum was assumed to be a broken PL and the index of the electron spectrum (p) below the break Lorentz factor was determined by the X-ray photon index as $p = 2\Gamma - 1 = 2.3$ and 2.0, in MWL I and MWL II, respectively. We obtained the following seven free parameters to describe the observed SED: the Doppler factor (δ), the electron energy density ($u_{\rm e}$), the magnetic field (B), the blob radius (R), and the minimum, break, and maximum Lorentz factor of the electrons ($\gamma_{\rm min}$, $\gamma_{\rm break}$, and $\gamma_{\rm max}$, respectively). Adopting the optical variability time scale ($T_{\rm var} \sim 4$ days; section 3.2) in MWL II, the relation between δ and R should be subjected to $R < cT_{\rm var}\delta/(1+z) = 1.2 \times 10^{17}(T_{\rm var}/4{\rm days})(\delta/15)$ cm where c and z are the speed of light and the redshift of the source, respectively.

We derived the SSC model parameters as summarized in table 6. The resultant model curves are shown with solid lines in figure 8. The both model predictions are well below the upper limit on the VHE γ-ray spectra. The SED in MWL I was reproduced with $\delta = 15$, $B = 0.71$ G, $R = 7.0 \times 10^{16}$ cm, $\gamma_{\rm min} = 70$, $\gamma_{\rm break} = 700$, $\gamma_{\rm max} = 3300$, and $u_{\rm e} = 1.5 \times 10^{-3}$ erg cm^{-3}. The δ and R are typical values for LBL (Ghisellini et al. 1998). On the other hand, in the SED in MWL II, the SSC model with $u_{\rm e} = 2.1 \times 10^{-3}$ erg cm^{-3} and $\gamma_{\rm max} = 4500$ was found to describe the SED successfully, while the other parameters remained unchanged. Thus, we adopt the interpretation that the increase in the electron energy density produced the second flare.

The SED spectra obtained in 1st and 2nd flare during 2005 – 2008 outburst are suggested to have different features as we saw in the X-ray spectra obtained with XMM-Newton and Suzaku. The difference in these SED spectra may require not only simple 'disk impact' (Valtonen et al. 2008a), but also a state transition of the disk - jet system (Valtaoja et al. 2000).

In 2008, Fermi successfully detected a γ-ray spectrum from the quiescent state of OJ 287 during its first three months (Abdo et al. 2009), as shown in figure 8. The measured γ-ray flux significantly exceeds our simple SSC model flux. This may indicate a contribution of external

Compton (EC) radiation to the γ-ray emission from OJ 287. Assuming that the γ-ray spectrum peaks around $\sim 1 \times 10^{22}$ Hz with a flux of $\sim 2 \times 10^{-11}$ erg s^{-1} cm^{-2}, as is suggested from figure 8, and using the electron spectrum determined from the SSC fitting to the radio-to-X-ray spectrum derived for MWL II, the energy density and typical frequency of $u_{\rm seed} \sim 10^{-5}$ erg cm^{-3} and $\nu_{\rm seed} \sim 10^{14}$ Hz in the rest frame of the nucleus (not the jet frame) are required for the seed photons of the EC process. These give the luminosity of the seed photon source as $\sim 10^{42}$ erg s^{-1}. This luminosity is consistent with that evaluated for 3C 279 (Inoue & Takahara 1996), a famous quasar-hosted blazar of which the γ-ray spectrum is thought to be dominated by the EC emission, within an order of magnitude. However, for a precise identification of the seed photon source, it is crucial to make a simultaneous multi-wavelength observation from radio to γ-ray frequencies.

5. Summary

We performed X-ray observations of OJ 287 in the quiescent state (MWL I) in 2007 April and in the flaring state (MWL II) in 2007 November by using Suzaku, together with radio, optical, and VHE γ-ray observations with NMA, KANATA, and MAGIC, respectively. The obtained results can be summarized as follows.

- The brightness of OJ 287 increased by a factor of 2 from MWL I with a 1 keV flux density of 215 ± 5 nJy to MWL II with 404^{+6}_{-5} nJy. The X-ray spectrum of OJ 287 was harder in MWL II (a photon index of $\Gamma = 1.50 \pm 0.01$) than in MWL I ($\Gamma = 1.65 \pm 0.02$).
- In MWL II, hard X-ray signals from the object were detected with a significance of 5.0σ in the 12 – 27 keV range, for the first time.
- The radio and optical fluxes doubled from MWL I to MWL II. No significant VHE γ-ray signals were detected in either observation.
- In both observations, the object exhibited a typical blazar-like spectral energy distribution consisting of synchrotron and inverse Compton components. The relative hard X-ray spectrum appeared to be dominated by the inverse Compton components.
- No significant difference of the synchrotron cut-off or peak frequency was found between the quiescent and flaring states. This spectral behavior is rather different from that in past flares, in which it appeared that the synchrotron component contributed to the X-ray spectrum.
- Based on the synchrotron self-Compton model, the change of the multi-wavelength spectral energy distribution is interpreted as the increase of the electron energy density, without any notable change in either the magnetic field or the electron Lorentz factor.

We thank all members of the Suzaku team for performing successful operatio and calibration. The Nobeyama Radio Observatory is a branch of the National Astronomical Observatory of Japan, the National Institutes of Natural Sciences (NINS). IRAF is distributed

by the National Optical Astronomy Observatories, which are operated by the Association of Universities for Research in Astronomy, Inc., under a cooperative agreement with the National Science Foundation. We would like to thank the Instituto de Astrofisica de Canarias for the excellent working conditions at the Observatorio del Roque de los Muchachos in La Palma. The support of the German BMBF and MPG, the Italian INFN and Spanish MICINN is gratefully acknowledged. This work was also supported by ETH Research Grant TH 34/043, by the Polish MNiSzW Grant N N203 390834, and by the YIP of the Helmholtz Gemeinschaft. Dr. J. Kataoka kindly provided valuable information on the numerical calculation for the wide-band spectrum of blazars. N. I. is supported by the Grant-in-Aid for the Global COE Program, "The Next Generation of Physics, Spun from Universality and Emergence" from the Ministry of Education, Culture, Sports, Science and Technology (MEXT) of Japan.

References

Abdo, A. A., et al. 2009, arXiv:0902.1559

Albert, J., et al. 2007, ApJ, 666, L17

Albert, J., et al. 2008a, ApJ, 674, 1037

Albert, J., et al. 2008b, Nucl. Instrum. and Meth., A588, 424

Aliu, E., et al. 2009, Astroparticle Physics, 30, 293

Bessell, M. S. 1979, PASP, 91, 589

Boldt, E. 1987, Observational Cosmology, 124, 611

Capetti, A., Celotti, A., Chiaberge, M., de Ruiter, H. R., Fanti, R., Morganti, R., & Parma, P. 2002, A&A, 383, 104

Ciprini S.,et al. 2008, in proceedings of Workshop on Blazar Variability across the Electromagnetic Spectrum, PoS(BLAZARS2008)030

Fiorucci, M., & Tosti, G. 1996, A&AS, 116, 403

Fossati, G., Maraschi, L., Celotti, A., Comastri, A., & Ghisellini, G. 1998, MNRAS, 299, 433

Fomin, V. P., Stepanian, A., A., Lamb, R. C., Lewis, D. A., Punch, M., & Weekes, T. C. 1994, Astropart. Phys., 2, 137

Fukazawa, Y., et al. 2009, PASJ, 61, 17

Ghisellini, G., Celotti, A., Fossati, G., Maraschi, L., & Comastri, A. 1998, MNRAS, 301, 451

Giommi, P., et al., 1999, A&A, 351, 59

Hillas, A. M. 1985, Proc. 29th Int. Cosmic Ray Conf. (La Jolla), 3, 445

Idesawa, E., et al. 1997, PASJ, 49, 631

Ishida et al. 2007, Suzaku Memo 2007-11

Ishisaki, Y., et al. 2007, PASJ, 59, 113

Isobe, N., Tashiro, M., Sugiho, M., & Makishima, K. 2001, PASJ, 53, 79

Inoue, S., & Takahara, F. 1996, ApJ, 463, 555

Kalberla, P. M. W., Burton, W. B., Hartmann, D., Arnal, E. M., Bajaja, E., Morras, R., Pöppel, W. G. L. 2005, A&A, 440, 775

Kataoka, J., Ph.D thesis, 2000, Univ. of Tokyo
Kidger, M. R. 2000, AJ, 119, 2053
Kokubun, M., et al. 2007, PASJ, 59, 53
Koyama, K., et al. 2007, PASJ, 59, 23
Kubo, H., Ph.D thesis, 1997, Univ. of Tokyo
Li, T.-P., & Ma, Y.-Q. 1983, ApJ, 272, 317
Mitsuda, K., et al. 2007, PASJ, 59, 1
Okumura, S. K., et al. 2000, PASJ, 52, 393
Padovani, P. & Giommi, P. 1995, ApJ, 444, 567
Pursimo, T., et al. 2000, A&AS, 146, 141
Rolke, W. A., Lopez, A. M., & Conrad, J. 2005, Nucl. Instrum. and Meth., A551, 493
Sambruna, R. M., Barr, P., Giommi, P., Maraschi, L., Tagliaferri, G., & Treves, A. 1994, ApJ, 434, 468
Serlemitsos, P. J., et al. 2007, PASJ, 59, 9
Shrader, C.R., Hartman, R.C., Webb, J.R., 1996, A&A, 120, 599,
Skiff, B. A., 2007, VizieR Online Data Catalog, 2277, 0
Skrutskie, M. F., Cutri, R. M., Stiening, R., Weinberg, M. D., Schneider, S., Carpenter, J. M., Beichman, C., Capps, R., et al. 2006, AJ, 131, 1163-1183
Stickel, M., Fried, J. W., & Kuehr, H. 1989, A&AS, 80, 103
Sillanpää, A., Haarala, S., Valtonen, M. J., Sundelius, B., & Byrd, G. G. 1988, ApJ, 325, 628
Sillanpää, A., et al. 1996, A&A, 315, L13
Sillanpää, A., et al. 1996, A&A, 305, L17
Takahashi, T., et al. 2000, ApJ, 542, L105
Takahashi, T., et al. 2007, PASJ, 59, 35
Teshima, M., et al. 2008, The Astronomer's Telegram, #1500
Valtonen, M. J., et al. 2006, ApJL, 643, L9
Valtonen, M., et al., 2008, Nature, 452, 7189, 851
Valtonen, M., Kidger, M., Lehto, H., & Poyner, G., 2008, A&A, 477, 407
Valtaoja, E., Teräsranta, H., Tornikoski, M., Sillanpää, A., Aller, M. F., Aller, H. D., & Hughes, P. A. 2000, ApJ, 531, 744
Madejski, G. M., & Schwartz, D. A. 1988, ApJ, 330, 776
Majumdar, P., Moralejo, A., Bigongiari, C., Blanch, O., & Sobczynska, D. 2005, in Proc. 29th Int. Cosmic Ray Conf. (Pune, India), 5, 203
Massaro, E., et al. 2003, A&A, 399, 33
Watanabe, M., et al. 2005, PASP, 117, 870

Table 1. Summary of model fitting to the Suzaku XIS spectra.

obs	Models	$N_{\rm H}$*	Γ	$S_{\rm 1keV}$†	Γ‡	$S_{\rm 1keV}$†‡	χ^2/d.o.f.	$F_{\rm 2-10keV}$§
MWL I	PL	2.56‖	1.65 ± 0.02	215 ± 5	–	–	215.0/243	1.44×10^{-12}
MWL II	PL	2.56‖	1.50 ± 0.01	404^{+6}_{-5}	–	–	566.3/520	3.42×10^{-12}
	double PL	2.56‖	$1.50^{+0.01}_{-0.02}$	404^{+4}_{-9}	2.62 (Fixed)	< 8.7	566.4/519	3.42×10^{-12}

* in 10^{20} cm^{-2}.
† X-ray flux density at 1 keV, in units of nJy.
‡ Soft PL component parameter.
§ 2 – 10 keV flux in erg cm^{-2} s^{-1}.
‖ Fixed at the Galactic Value.

Table 2. Event statistics of the HXD data in MWL I.

	Earth occulation		On-source	
	12 – 20 keV	20 – 40 keV	12 – 20 keV	20 – 40 keV
Data (c s^{-1})	0.274 ± 0.003	0.149 ± 0.002	0.319 ± 0.002	0.173 ± 0.001
NXB (c s^{-1})	0.264 ± 0.001	0.150 ± 0.001	0.290 ± 0.001	0.167 ± 0.001
CXB (c s^{-1})	–	–	0.016	0.008
excess (c s^{-1})*	0.010 ± 0.003	-0.015 ± 0.002	0.012 ± 0.002	-0.002 ± 0.001
excess* ratio† (%)	3.8 ± 1.0	-1.0 ± 1.3	4.2 ± 0.3	-0.9 ± 0.2

* Data excess over the NXB and the combined NXB and CXB for Earth occultation and on-source, respectively.
† Ratio to the NXB model.

Table 3. The event statistics of the HXD data in MWL II.

	Earth occultation		On-source
	12 – 20 keV	20 – 40 keV	12 – 27 keV
Data (c s^{-1})	0.286 ± 0.003	0.165 ± 0.002	0.399 ± 0.002
NXB (c s^{-1})	0.290 ± 0.001	0.167 ± 0.001	0.367 ± 0.001
CXB (c s^{-1})	–	–	0.022
excess (c s^{-1})*	-0.004 ± 0.003	-0.002 ± 0.003	0.011 ± 0.002
excess* ratio†	-1.4 ± 1.2	-1.2 ± 1.6	2.9 ± 0.6

* Data excess over the NXB and the combined NXB and CXB for Earth occultation and on-source, respectively.
† Ratio to the NXB model.

Table 4. Summary of radio and optical fluxes obtained during the Suzaku pointing in MWL I and MWL II.

obs	radio flux (Jy)		optical flux (mJy)			
	86.95 GHz*	98.75 GHz*	K_s †	J †	R ‡	V†
MWL I	1.73 ± 0.26	1.75 ± 0.26	17.74 ± 0.33	8.82 ± 0.03	3.20 ± 0.05	3.03 ± 0.01
MWL II	3.04 ± 0.46	2.98 ± 0.46	$55.95^{+7.69}_{-6.76}$	27.02 ± 0.21	8.70 ± 0.14	8.93 ± 0.05

* NMA data.
† KANATA data.
‡ KVA Telescope data.

Table 5. Results of the search for VHE γ-ray emissions from OJ 287.

MWL I			
Threshed Energy (GeV)*	80	145	310
ON events†	40056	1219	42
OFF events‡	40397 ± 226	1340 ± 38	39.5 ± 6.3
significance (σ)§	-1.13	-0.94	-0.47
U.L. of excess events‖	394	75.1	21.9
$\mathrm{Flux}_{95\%\mathrm{U.L.}}$ ($\times 10^{-12}$ cm^{-2} s^{-1})#	59.8	11.1	2.83
Crab Flux(%)**	8.5	3.3	2.4
MWL II			
Threshed Energy (GeV)*	85	150	325
ON events†	281885	12582	578
OFF events‡	282342 ± 493	12573 ± 65	576 ± 14
significance (σ)§	-0.75	0.07	0.07
U.L. of excess events‖	1218	330	71.6
$\mathrm{Flux}_{95\%\mathrm{U.L.}}$ ($\times 10^{-12}$ cm^{-2} s^{-1})#	22.1	5.64	1.18
Crab Flux(%)**	3.4	1.7	1.1

* Correspond to peak energies of γ-ray Monte Carlo samples after all cuts.
† Number of measured ON events.
‡ Normalized number of OFF events and related error.
§ Based on equation (17) in Li & Ma (1983),
‖ 95% upper limit of the number of excess events with 30% systematic error.
Flux upper limit assuming a photon index of -2.6 for the calculation of the effective area.
** Corresponding Crab flux in each energy range based on measurements of the Crab pulsar performed with the MAGIC telescope (Albert et al. 2008a)

Table 6. Physical parameters for the SSC model.

parameters*	MWL I	MWL II
δ	15	
R (cm)	7.0×10^{16}	
B (Gauss)	0.71	
γ_{min}	70	
γ_{break}	700	
γ_{max}	3300	4500
p	2.3	2.0
u_{m} (erg cm^{-3})	2.0×10^{-2}	2.0×10^{-2}
u_{e} (erg cm^{-3})	1.5×10^{-3}	2.1×10^{-3}

* Notations are described in the text.

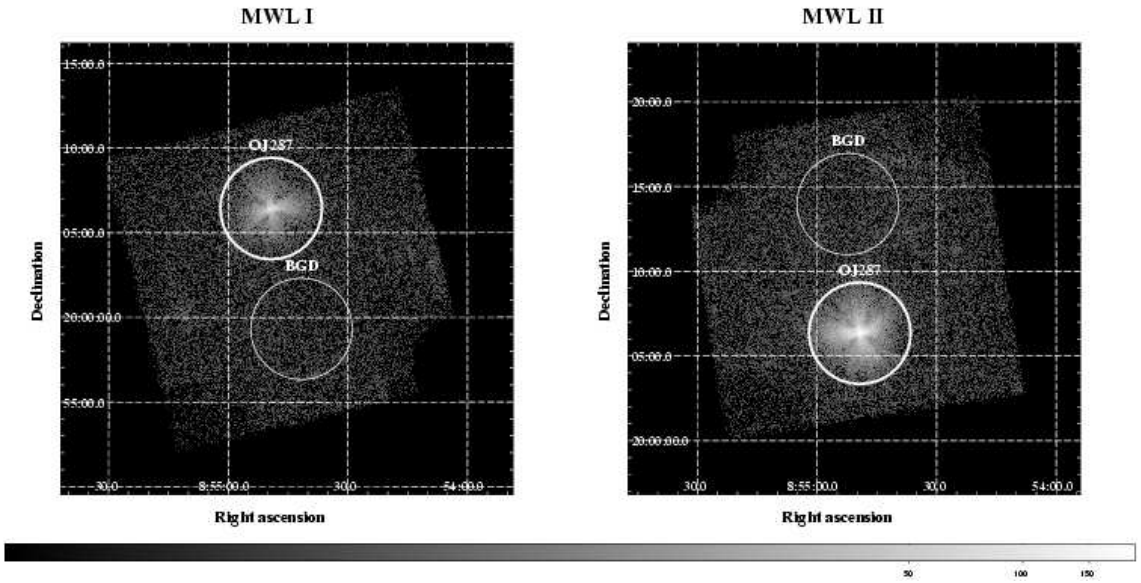

Fig. 1. The 0.5 – 10 keV XIS image of OJ 287 in MWL I (left) and MWL II (right). Data from all XIS CCD chips (XIS 0, 1, and 3) were summed up. The region of the calibration sources was removed. Background subtraction and exposure correction are not applied to the image. Both panels are drawn in the same grayscale. The source and the background signals are integrated within the solid and dashed circles, respectively.

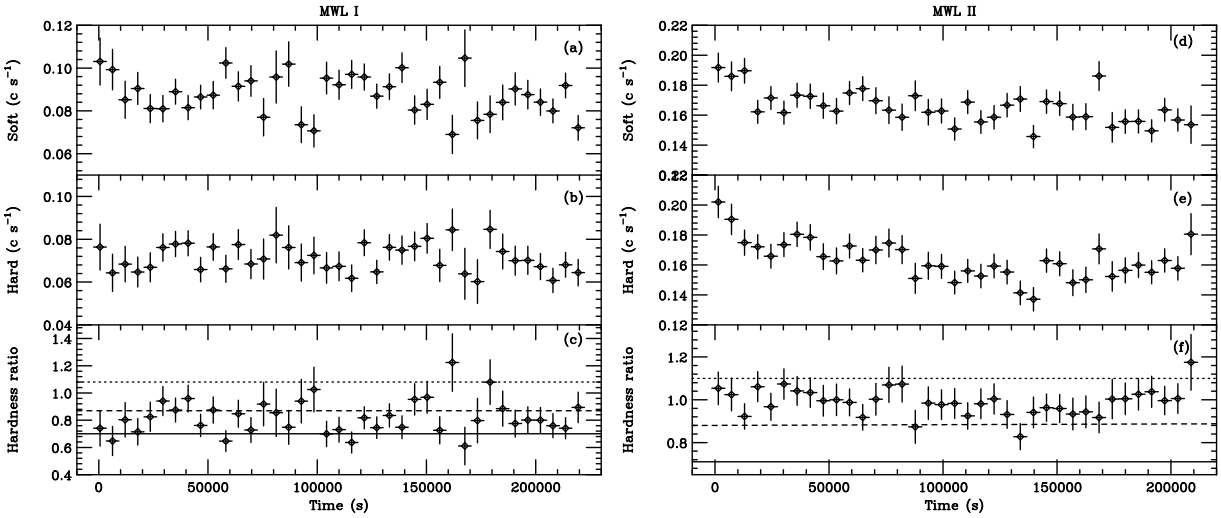

Fig. 2. The XIS FI lightcurves of OJ 287 obtained in MWL I and MWL II. The time bin was set to 5760 s. Panels (a) and (d) show the soft energy band lightcurves (0.5 – 2 keV), while panels (b) and (e) show the medium energy band lightcurves (2 – 10 keV) in each observation. The hardness, which is simply calculated as the ratio of the hard band count rate to the soft band one, is shown in panels (c) and (f). The dotted, the dashed, and the solid lines in panels (c) and (f) indicate the predictions provided by the PL model with Γ=1.4, 1.6, and 1.8, respectively.

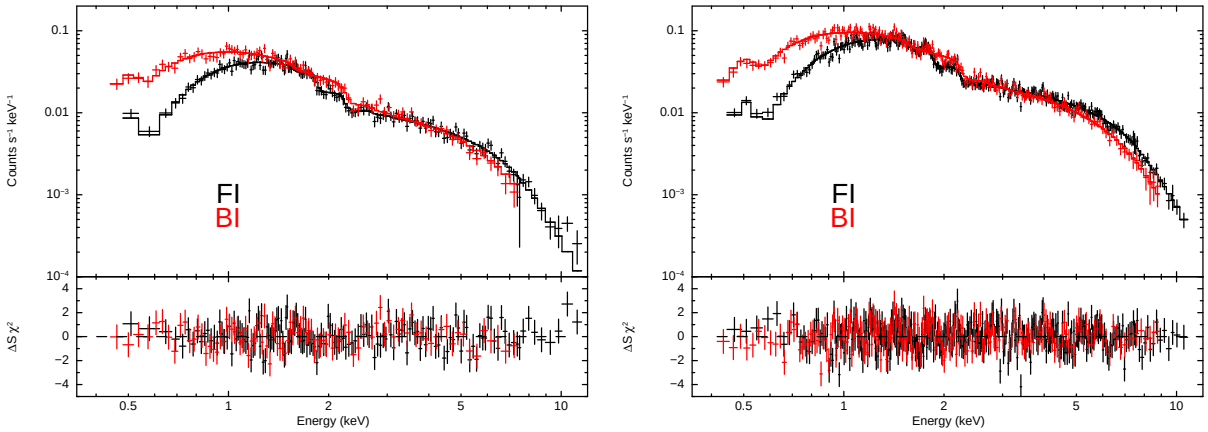

Fig. 3. The XIS spectra of OJ 287 in MWL I and MWL II. The FI and BI data are shown with black and red points, respectively. The data are binned into pixels with at least 100 events, and error bars represent 1 σ statistical errors. Histograms in both panels indicate the best-fit PL models.

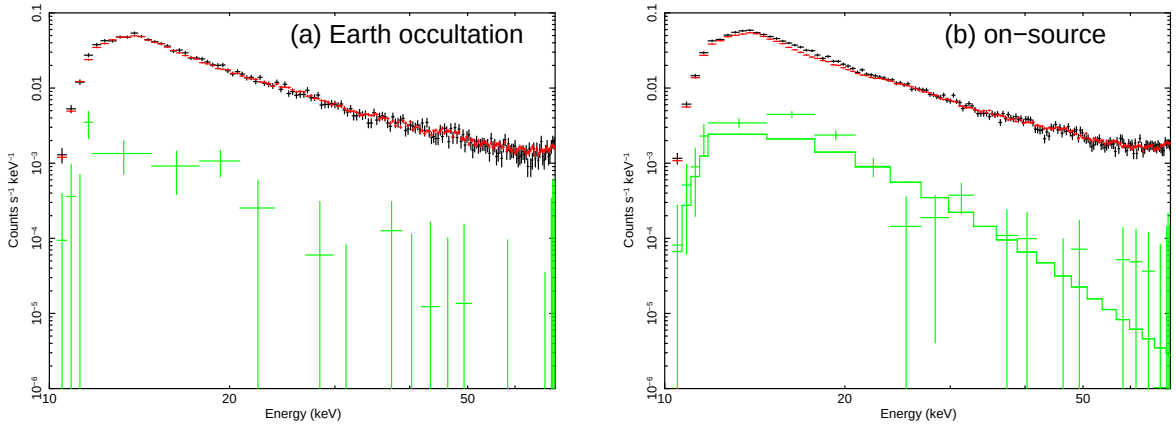

Fig. 4. The HXD-PIN spectra of OJ 287 in MWL I, obtained in the Earth occultation (panel a) and the on-source observations (panel b). The black, red, and green data points indicate the data, NXB model, and NXB-subtracted spectra, respectively. The green histogram in panel (a) shows the CXB model spectrum (see the text).

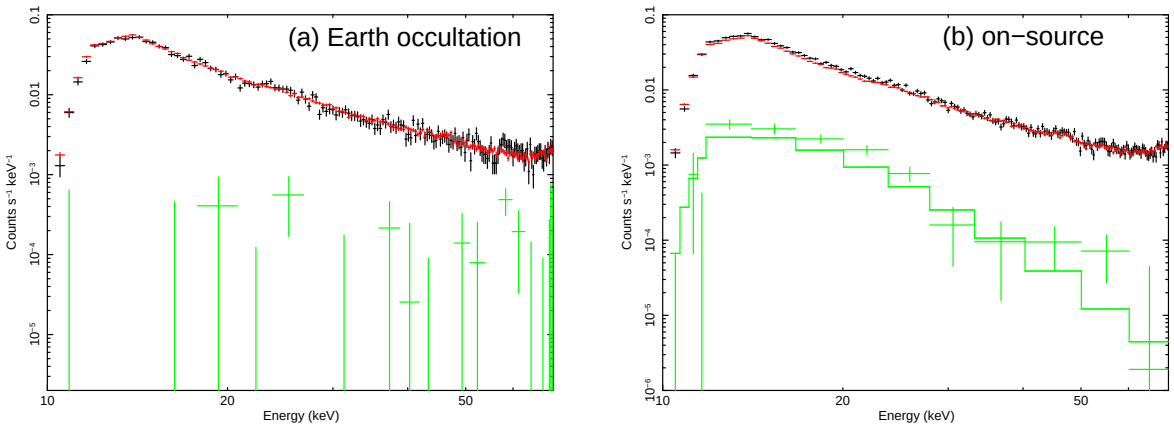

Fig. 5. The HXD-PIN spectra of OJ 287 in MWL II, presented in the same manner as in figure 4.

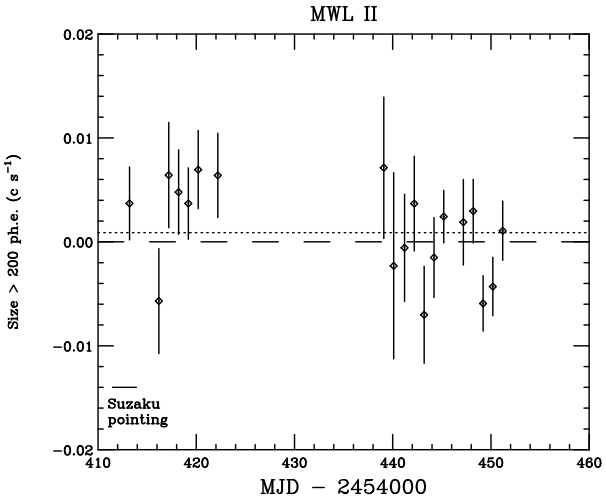

Fig. 6. Excess event rate with SIZE above 200 photoelectrons (with a corresponding energy threshold of 150 GeV), observed with the MAGIC telescope in MWL II. The dotted line indicates the average count rate.

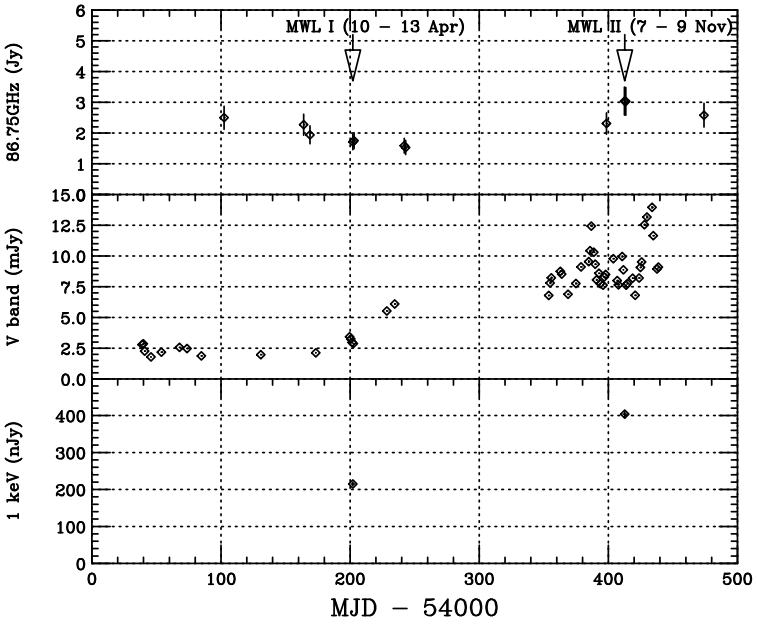

Fig. 7. The multi-wavelength lightcurves of OJ 287. The top panel shows the radio flux at 86.75 GHz as observed with NMA, while the middle panel shows the optical flux in the V-band as observed with KANATA. The radio and optical fluxes are averaged over each night. The bottom panel shows the X-ray flux density at 1 keV. Arrows indicate the Suzaku pointings in MWL I and MWL II.

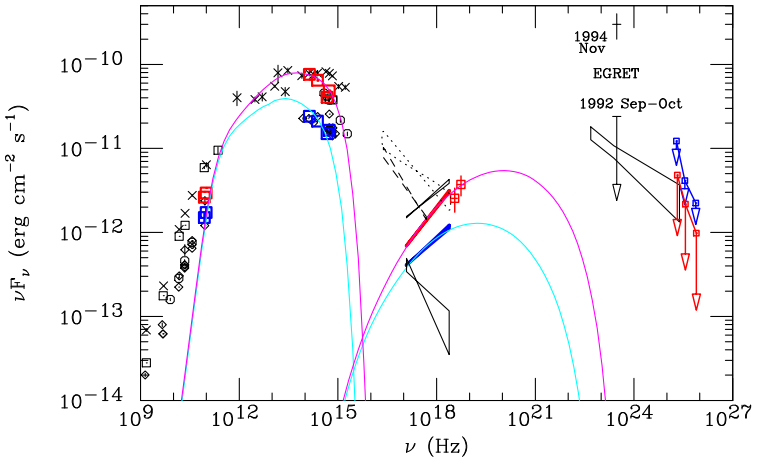

Fig. 8. The SED of OJ 287 during the Suzaku observations in MWL I (blue) and MWL II (red). The radio and optical data are shown with squares and, the X-ray data are shown with bow ties. The upper limit of the VHE γ-ray spectrum are measured values, shown with downward arrows. The light blue lines and the purple lines indicate the simple one-zone SSC model for MWL I and MWL II, respectively. The black data points show radio, optical, and γ-ray data from non-simultaneous observations. The X-ray spectra with EXOSAT, ROSAT, and ASCA are drawn with dotted, dashed, and solid lines, respectively (Idesawa et al. 1997; Isobe et al. 2001 and references therein). The γ-ray spectrum obtained with Fermi during the first 3 month observation (August – October 2008) is shown with a bow tie (Abdo et al. 2009).